International Forum on Aeroelasticity and Structural Dynamics
IFASD 2019
9-13 June 2019, Savannah, Georgia, USA

# FLUTTER MECHANISMS CHARACTERIZATION USING DISTRIBUTED AEROELASTIC ENERGY ANALYSIS

**Cap. Yaara Karniel and Cap. Daniel Kariv and Maj. Michael Iovnovich**[1]

[1]Flight Sciences Branch
Israeli Air Force
Tel-Aviv, Israel
smichael.iov@gmail.com

**Keywords:** Flutter analysis, Distributed aeroelastic energy, Flutter mechanism, Fighter aircraft flutter

**Abstract:** The problem of flutter mechanism classification is important particularly for modern fighter aircrafts, for which the amount of aircraft configurations which require analysis is typically large. Common flutter mechanism classification and characterization techniques rely on characteristics which represent the structural motions at flutter conditions rather than a quantitative measure of the instability severity or its origins. Such classifications may be somewhat subjective, require tedious treatment by the analyst and may in some cases lead to wrong conclusions. The current study aims to enhance flutter mechanism characterization and classification processes by using an aeroelastic energy balance analysis which is formulated in structural coordinates. The method may be easily applicable to typical industrial flutter analysis data and enables to identify distributed aeroelastic energy patterns which are visualized on the configuration structural model. This analysis approach is shown to enable straightforward identification of the structural parts which are the dominant contributors to the unstable coupling and thereby to distinguish between physically dissimilar flutter cases. The application of aeroelastic energy-based parameters for flutter mechanism classification is presented in this study for a representative dataset including thousands of wing flutter cases of the F-16 aircraft with various stores. Using the suggested approach, six basic flutter mechanism groups are identified in the examined dataset. Over 98% of the examined flutter cases may be automatically classified to one of these mechanism groups, which demonstrates the potential of this approach.

## 1 INTRODUCTION

Flutter instability of flexible aerodynamic structures occurs as the unsteady aerodynamic forces interact with the structural elastic and inertial forces, yielding an unstable aeroelastic dynamic system. From a thermodynamic perspective, such systems are nonconservative in nature and require for an energy transfer from the airstream and into the structure to take place. Once flutter onset flow conditions are exceeded, energy is continuously pumped into the structure such that the structural response amplitudes are ever increasing until failure is reached. The aeroelastic energy balance is broadly discussed in aeroelastic textbooks and commonly evaluated in flutter-related energy harvesting and turbomachinery applications, however, it is seldom indicatively used during industrial aircraft flutter investigations.

A typical aircraft flutter assessment includes a stability analysis of all relevant aircraft configurations and a dedicated investigation of several representative configurations in ground vibration

tests and flutter flight tests. While for civil aircrafts the set of flutter configurations may typically consist of a few dozens of cases, modern fighter aircrafts are usually characterized by considerably larger configuration sets [1]. This is mainly due to the vast diversity of weapon/store inventory and the introduction of asymmetric configurations throughout the mission due to fuel consumption, weapon employment, etc. To reduce the complexity of fighter aircraft flutter analysis investigations, a common methodology aims to divide the overall analyzed flutter cases into a subset of several groups, with each group including all flutter cases sharing a similarity in its flutter mechanism. This classification into basic flutter mechanism groups enables the engineer to characterize each mechanism and to identify the critical flutter cases in each mechanism which shall be further addressed during the following flutter clearance activities. The evaluation of mechanism similarity between two different flutter cases is conducted based on a set of *flutter characteristics*, which typically include the flutter mode frequency, flutter coupling natural mode shapes and corresponding frequencies and the aeroelastic modal damping and frequency curves trends with dynamic pressure. The flutter mode, which represents the structural oscillatory motion at flutter onset conditions, may also be used to identify key features such as the symmetry conditions and phase lag between bending and torsion/pitch motions. A classification process based on such characteristics may be somewhat subjective or even ad-hock, as it is ultimately impossible to identify absolute criteria for distinguishing between two different mechanisms. Consequently, such a process is time consuming and requires special attention by the engineer if performed manually. Livshitz and Iovnovich [2] developed an artificial neural network based machine learning algorithm which probabilistically classifies a flutter case into pre-supervised mechanisms using the flutter mode motions at several structural locations. The algorithm is trained on manually classified datasets and was demonstrated to enable successful classifications of rather simple flutter cases, while low confidence classifications still require manual evaluation. One drawback of using the flutter mode as the principal flutter characteristic for mechanism classification is that it represents the resultant structural response due to the unstable coupling, rather than the origins of the instability. Additionally, the flutter mode structural motions are insufficient to quantitatively measure the severity of the instability. An aeroelastic energy balance assessment may be used to calculate the unstable contributions of the various acting forces and split these contributions between different structural elements, and therefore may significantly enhance both manual and automated flutter mechanism classification processes.

In a recent study by Ricciardi [3], the aerodynamic work per single flutter mode cycle was integrated based on typical flutter analysis results and visualized on the aerodynamic model. This visualization was shown effective in identifying regions across the aerodynamic surfaces which are characterized with positive energy balance per cycle and therefore invoke the unstable coupling. The aerodynamic work surface patterns were then used to identify various system stability conditions and to compare between different flutter cases.

The current paper further develops Ricciardi's work by analyzing the overall distributed aeroelastic energy balance at flutter conditions. The analysis is formulated in structural coordinates and conducted in terms of average aeroelastic power per normalized amplitude flutter mode cycle. This formulation enables to take the local kinetic (inertial forces) and potential (elastic forces) energies into account, and visualize the distributed aeroelastic power on the structural model. The F-16 fighter aircraft is used as a test case in order to demonstrate how the suggested analysis may enhance flutter investigations and support flutter mechanism characterization and classification on the industrial level.

## 2 THEORETICAL MODEL

The aeroelastic equations of motion in structural coordinates may be written as:

$$[M]\{\ddot{X}\} + [C]\{\dot{X}\} + [K]\{X\} = \{F_a\} \tag{1}$$

Where $[M]$, $[C]$, and $[K]$ are the structural mass, damping and stiffness matrices respectively, and $\{X\}$ is the vector of structural displacements. $\{F_a\}$ is the vector of aerodynamic forces, which is time variant, and depends on the flow conditions and on the structural displacements. Using the modal approach, the structural displacements may be written as a linear combination of the elastic modes of the wing such that:

$$\{X\} = [\phi]\{\xi\} \tag{2}$$

Where $[\phi]$ is the modes matrix in which every column represents a mode shape in structural coordinates, and $\{\xi\}$ are the elastic generalized displacements. Assuming harmonic oscillatory motion of $\omega$ frequency at flutter onset conditions we obtain:

$$\{\xi\} = \{\xi_0\}e^{i\omega t} \tag{3}$$

$$\{X\} = \{X_0\}e^{i\omega t} \tag{4}$$

where $\{\xi_0\}$ and $\{X_0\}$ are complex amplitude vectors. The displacement time variation at structural degree of freedom (DOF) $i$ can also be written as:

$$x_i = \overline{x}_i cos(\omega t + \psi_i) \tag{5}$$

where $\overline{x}_i$ is the motion absolute amplitude and $\psi_i$ is the motion phase with respect to the motion of other DOFs. Reforming Eq. (1) in generalized coordinates leads to the modal-coordinates aeroelastic equations of motion:

$$[GM]\{\ddot{\xi}\} + [GC]\{\dot{\xi}\} + [GK]\{\xi\} = \{GF_a\} \tag{6}$$

where $[GM] = [\phi]^T[M][\phi]$, $[GC] = [\phi]^T[C][\phi]$, and $[GK] = [\phi]^T[K][\phi]$ are the generalized mass, damping and stiffness diagonal matrices, respectively. While $[\phi], [GM]$ and $[GK]$ can be calculated from a finite element model of the structure, the structural damping is usually unknown and modeled as:

$$GC_i = g_i\omega_i GM_i \tag{7}$$

where $GC_i$ is the i-th element on the generalized damping matrix diagonal, $\omega_i$ is the modal frequency and $g_i$ is the structural damping coefficient, which is assumed to be in the range of

$g_i = 0.5 - 2.5\%$. The vector of generalized aerodynamic forces, $\{GF_a\}$, is computed according to:

$$\{GF_a\} = [\phi]^T\{F_a\} \tag{8}$$

When using a panel method unsteady aerodynamics model, the so-called aerodynamic influence coefficient ($[AIC]$) matrix is computed per Mach number and reduced frequency $k = \omega L/V$ conditions, where $L$ is a reference length and $V$ is the airflow velocity. This matrix represents the unsteady aerodynamic force response in each panel due to unit amplitude harmonic deflection of each of the other panels in the model. The $[AIC]$ matrix may be transferred from the aerodynamic model coordinates into the structural model coordinates using the spline transformation matrix $[G]$. $\{F_a\}$ may then be computed according to:

$$[AFC(ik)] = [G]^T[AIC(ik)][G] \tag{9}$$

$$\{F_a(ik)\} = [AFC(ik)]\{X\} \tag{10}$$

During a typical flutter analysis, Eq. (6) is solved as a complex stability eigenproblem according to flutter solver formulations such as the G method [4]. Once flutter onset conditions are identified, the complex oscillatory flutter mode $\{\xi_f\}$ and flutter mode frequency $\omega_f$ may be extracted and transformed into structural coordinates according to Eq. (2), where the flutter mode is represented by $\{X_f\}$. By time-differentiating $\{X_f\}$ into $\{\dot{X}_f\}$ and $\{\ddot{X}_f\}$, the terms of the oscillatory inertial, stiffness (see Eq. (1)) and aerodynamic (see Eq. (10)) forces during a single flutter mode cycle may be obtained by:

$$\{I_f\} = -\omega_f^2[M]\{X_f\} \tag{11}$$

$$\{K_f\} = [K]\{X_f\} \tag{12}$$

$$\{A_f\} = [AFC]\{X_f\} \tag{13}$$

The work per time carried by each structural DOF equals the sum of forces acting on the DOF times the DOF deflection velocity. Defining positive work as the work which transfers energy into the structure (i.e. damping/dissipation energy) and negative work as the work carried by the structure we obtain:

$$\{W\} = \{F_{tot}\} \cdot \{\dot{X}_f\} \tag{14}$$

$$\{F_{tot}\} = \{A_f\} - (\{K_f\} + \{I_f\}) \tag{15}$$

Similarly to Eq. (5), the deflection velocity and total force time variations at DOF $i$ equal:

$$f_{tot_i} = \overline{f}_{tot_i} cos(\omega_f t + \phi_i) \tag{16}$$

$$\dot{x}_{f_i} = -\omega_f \overline{x}_{f_i} sin(\omega_f t + \psi_i) \tag{17}$$

Therefore, the average aeroelastic power per flutter mode cycle (PPC) may be integrated for each DOF according to:

$$PPC_i = \frac{1}{T}\int_0^T f_{tot_i}\dot{x}_{f_i}dt = \frac{\pi}{T}\overline{x}_{f_i}\overline{f}_{tot_i} sin(\phi_i - \psi_i) \tag{18}$$

where $T = 2\pi/\omega_f$ is the flutter mode cycle period time. It is observed that Eq. (18) yields positive values (i.e. the structural DOF absorbs energy) if and only if $0 < \phi_i - \psi_i < \pi$, which corresponds with the classic flutter requirement according to which the force must lead

the displacement at unstable conditions. To obtain comparable power calculations between various configurations, the flutter mode shall be normalized to a maximum unit deflection. The sum of average aeroelastic PPC for a particular structural element or the entire aircraft may be calculated by summation of the relevant DOFs power.

When attempting to perform flutter mechanism characterization based on the flutter mode motions, the phase shift between wingtip torsion and bending motions may be used as an indicator for the force to motion phase requirement. The rational for using this parameter is that the aerodynamic forces act mainly normal to the aerodynamic surface and therefore primarily lead to bending motions, while variations of the aero forces are strongly correlated with torsional deflection through changes of the angle of attack along the wingspan. In the current study, the torsion to bending phase angle is defined as follows:

$$x_{torsion} = x_{LE} - x_{TE} \tag{19}$$

$$x_{bending} = 0.5(x_{LE} + x_{TE}) \tag{20}$$

$$\Theta_{T/B} = 90^\circ - [\angle(x_{torsion}) - \angle(x_{bending})] \tag{21}$$

where $x_{LE}$ and $x_{TE}$ are the wingtip leading edge and trailing edge motions, respectively. In these terms, the requirement for an unstable coupling is $-90^\circ < \Theta_{T/B} < 90^\circ$. This formulation is only an approximation to the proper requirement which is embedded into the aeroelastic power calculation.

## 3 TEST CASES

The F-16 fighter model is used as a test case for the purposes of the current study. Figure 1 presents the store configurations that were analyzed. The configurations include a full or empty fuel tank at the centerline station (St. 5), two types of fuel tanks at five possible fuel states (full to empty) at the inboard wing stations (St. 4/6), 12 various stores at the mid-span stations (St. 3/7), two types of missiles at the outboard wing stations (St. 2/8) and two types of missiles at the wingtip stations (St. 1/9). Overall, this configurations set includes 2592 symmetric permutations. All configurations were analyzed at Mach 0.95 and Mach 1.2, which yielded about 7000 flutter cases.

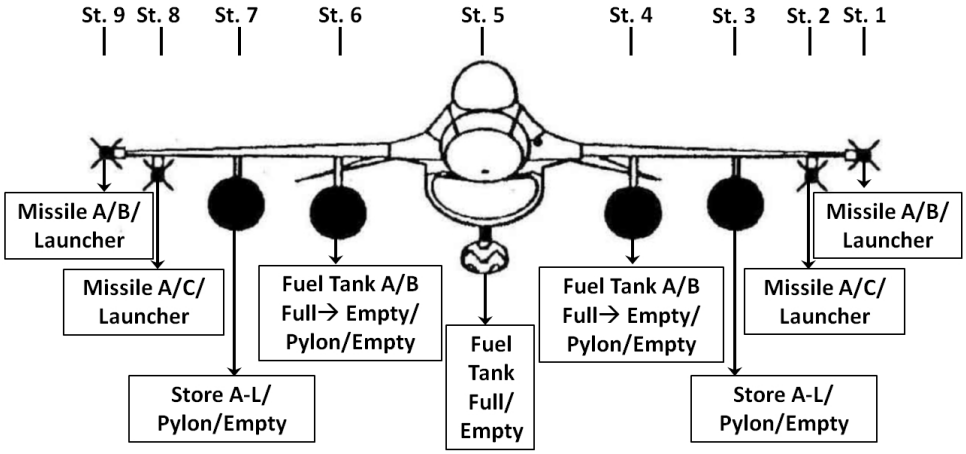


Figure 1: F-16 test case store configurations

The F-16 aeroelastic model is built from a structural finite element model (FEM) and a panel aerodynamic model. The FEM is a general element type of model which consists of stiffness

and inertia matrices for the different structural parts of the aircraft (fuselage, wing, stores, etc.). Some of the stores are represented as a point mass, while more elastic stores are represented by a stick model. The structural model is presented in Figure 2a. In the current study, a full-span structural model with natural modes of up to 25 Hz of frequency was used. All mode shapes are normalized to meet a unit maximum deflection. The F-16 aerodynamic model is a panel model that was generated and analyzed using the ZEARO software [5]. The model is presented in Figure 2b for a representative configuration. For most of the configurations used in this study, the AFC matrix includes external stores effects, therefore these effects are also included in the aeroelastic energy analysis.

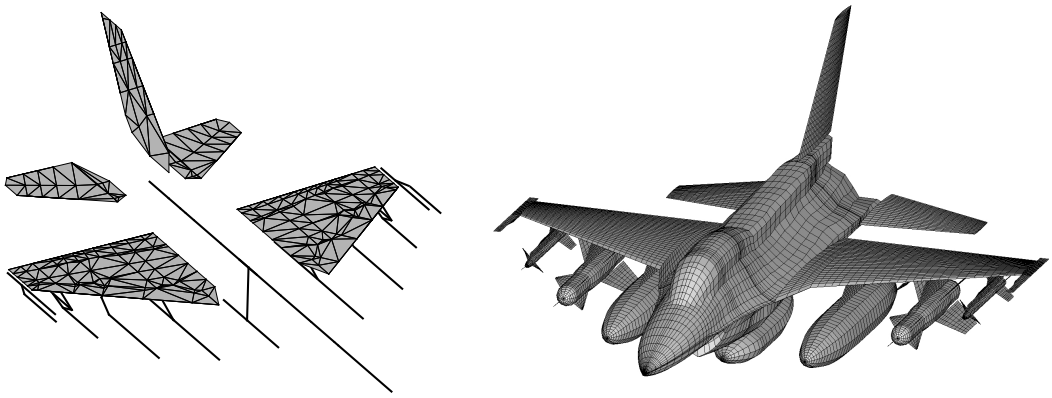

(a) FEM model (b) Aerodynamic model

Figure 2: F-16 fighter FEM dynamic and DLM aerodynamic models

## 4 RESULTS

### 4.1 Aeroelastic Energy Distributions

In this section, results are presented for seven representative flutter cases that were selected from the full dataset to demonstrate typical aeroelastic energy distribution results. Table 1 details the presented configurations. Table 2 presents typical flutter mechanism characterization data including Mach number, mechanism symmetry conditions, flutter mode frequency, normalized equivalent flutter onset airspeed and the phase angle between torsion and bending motions at the wingtips, which is computed according to Eq. (21). Flutter cases 1-5 are typical wing flutter cases of the F-16. Flutter case 6 is a vertical tail (VT) flutter case and case 7 is not a physical flutter case but an aeroelastic mode at stable conditions, which is used for demonstration purposes. From Table 2 it is observed that the wingtip torsion to bending phase requirement of $-90^\circ < \Theta_{T/B} < 90^\circ$ is maintained for cases 1-5, while for cases 6 and 7 this parameter indicates that no wing flutter is predicted. Also it is indicated that $\Theta_{T/B}$ is not correlative to the flutter onset speeds.

| Case | 1 | 2 | 3 | 4 | 5 | 6 | 7 |
|---|---|---|---|---|---|---|---|
| St. 1/9 | Launcher | Missile B | Launcher | Launcher | Launcher | Missile B | Missile B |
| St. 2/8 | Missile C | Missile C | Missile C | Launcher | Launcher | Missile C | Launcher |
| St. 3/7 | Store L | Store L | Store G | Store L | Store A | Store A | Store H |
| St. 4/6 | 1/3 Full Tank A | Empty Store | 1/3 Full Tank B | Full Tank B | Full Tank A | Empty Store | Full Tank B |
| St. 5 | Empty tank | Empty tank | Empty tank | Empty tank | Full Tank | Full tank | Full Tank |

Table 1: Description of test cases configurations

| Flutter Case | 1 | 2 | 3 | 4 | 5 | 6 | 7 |
|---|---|---|---|---|---|---|---|
| Mach | 0.95 | 0.95 | 0.95 | 0.95 | 0.95 | 1.2 | 1.2 |
| Symmetry | A/S | A/S | A/S | SYM | A/S | A/S | A/S |
| Freq. [Hz] | 5.6 | 4.3 | 6.7 | 5.3 | 7.0 | 14.1 | 5.9 |
| Norm. Flutter Speed | 6.9 | 6.6 | 3.8 | 6.6 | 6.1 | 11.6 | - |
| $\Theta_{T/B}$ [deg] | 36 | 51 | 48 | 50 | 31 | 233 | 246 |

Table 2: Test cases mechanism characterization based on flutter analysis results

Table 3 presents numeric results from the aeroelastic energy analysis at flutter conditions. The results include the total PPC (TPPC) of the entire aircraft model and the relative contributions of various structural parts to the TPPC. The structural parts' contributions are normalized by the contribution of the structural part with the maximum absolute PPC. The aeroelastic energy distributions are visually presented in Figure 3 for each of the flutter cases. In these plots, a maximum deflection snapshot from the flutter mode cycle is presented to demonstrate the structural deflection relations. Stores, missiles and missile launchers are represented by their structural body lines. The tip missiles are represented by two grid points, one in the middle and one in the nose of the missiles body, therefore, the tip missiles are visualized as they are mounted on the forward part of the tip launchers. The model is colored by PPC for each grid point, which is computed by summing all available DOFs PPC at each structural grid point. All PPC data is normalized by the highest PPC level among all test cases to allow comparison between the plots. Stores are colored by a uniform color which represents the overall store DOFs PPC. In these representations, negative PPC values represent stabilizing energy balance. The energy balance on a particular structural part or grid point may be higher than the TPPC, since it may be compensated by another part with negative energy balance. Focusing on the TPPC data presented in Table 3, the total power is in fact positive for flutter cases 1-6 which are valid flutter cases. As expected, the TPPC is negative for flutter case 7 which represents an aeroelastic mode at stable conditions. Similarly to $\Theta_{T/B}$, the TPPC is not correlative to the flutter onset speeds, suggesting that an energetic flutter mechanism may occur at both high or low dynamic pressure conditions. Generally, the presented flutter cases differ in its TPPC, as well as the energy distributions, which may aid in characterization of its flutter mechanisms. In most of the cases, a high positive PPC is identified at the leading edge region of the outboard wing. This is in agreement with the findings of Ricciardi [3] for both a rectangular Goland wing and an F-16 configuration. This result is also intuitive with a basic aeroelastic consideration according to which aerodynamic forces which act forward to a wing elastic axis (which is typically around the center of the wing chord) have diverging aeroelastic contribution to the system stability conditions. Furthermore, distinct differences in the contributions of the various store stations to the TPPC may be observed as follows. Flutter case 1 is considerably contributed by a positive outboard wing PPC (see Table 3), while the store stations contribute small or negative PPCs. Flutter case 2 is characterized with high PPCs at the tip missiles (see Figure 3b), which exhibit relative rotation motions with respect to the wingtip. Interestingly, this is the only flutter case where the outboard wing leading edge region does not contribute significant positive PPC. In flutter case 3, the outboard wing stores stations (2/8) seem to contribute positive PPC (see Figure 3c), however the overall contribution of the 2/8 stations is low in comparison with the outboard wing, as indicated in Table 3. Flutter case 4 is mainly contributed by the positive PPC of the mid-span stations (3/7), as indicated in Table 3 and in Figure 3d. Flutter case 5 is dominated by the inboard wing stations (4/6). This flutter case is characterized with significant lateral motion of the fuel tanks at stations 4/6. Flutter case 6 involves empennage bending-

torsion motions, and consequently characterized by high VT PPC levels, (see Figure 3f). Even though this is a VT flutter case, the outboard wing contributes positive PPC to this mechanism energy balance. Flutter case 7, which represents a stable aeroelastic mode, is characterized with small or negative contributions from most of the structural parts.

| Flutter Case | 1 | 2 | 3 | 4 | 5 | 6 | 7 |
|---|---|---|---|---|---|---|---|
| Total Power[W/m] | 167.8 | 113.1 | 138.1 | 1057.0 | 550.88 | 489.2 | -176.3 |
| Outboard Wing [%] | 100 | 40 | 100 | 74 | 80 | 100 | -9 |
| Midspan Wing [%] | 8 | -11 | 0 | -4 | 13 | 58 | 15 |
| Inboard Wing [%] | -45 | -22 | -33 | -21 | -6 | 22 | 38 |
| St. 1/9 [%] | 10 | 100 | 10 | -2 | -5 | -94 | 0 |
| St. 2/8 [%] | 12 | -16 | 51 | -19 | -28 | -39 | -7 |
| St. 3/7 [%] | 11 | -27 | 12 | 100 | -30 | 20 | 9 |
| St. 4/6 [%] | -18 | 0 | -7 | -55 | 100 | 0 | -5 |
| St. 5 [%] | -8 | -3 | -8 | 2 | -1 | -5 | -100 |
| Fuselage [%] | -62 | -25 | -91 | -17 | -37 | -8 | 38 |
| Horizontal Tail [%] | -7 | -4 | -6 | -1 | -3 | -23 | -7 |
| Vertical Tail [%] | -1 | -1 | -1 | 0 | 0 | 16 | -39 |

Table 3: Aeroelastic energy balance analysis results for various aircraft structural parts

By decomposing the aeroelastic forces in Eq. (15), it is possible to assess the aerodynamic, elastic and inertial PPC contributions. This decomposition is presented in Figure 4 for flutter case 1. The elastic and inertial forces are conservative and therefore their overall contribution to the TPPC is zero. Nevertheless, local stabilizing or destabilizing contributions may affect the energy distributions since PPCs due to these forces are not necessarily zero locally (on a grid point level). Furthermore, the inclusion of the elastic and inertial forces to the aeroelastic energy balance may affect the mechanism characterization, as demonstrated in Figure 4 for the elastic forces. From this presentation it is observed that the aerodynamic positive PPC contribution is mainly localized at the outboard wing region. The elastic contributions are mainly positive for 2/8 and 4/6 store stations and negative for the 4/6 station and wingtip stores. The inertial force contribution is more than 9 orders of magnitude smaller than the elastic and aerodynamic parts.

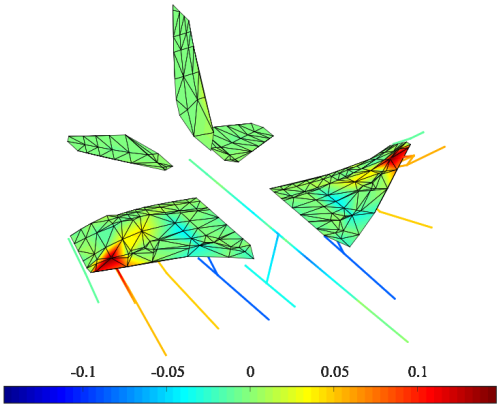


(a) Case 1, TPPC=167.8 W/m

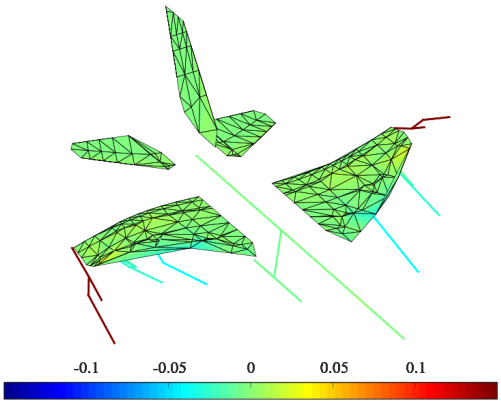


(b) Case 2, TPPC=113.1 W/m

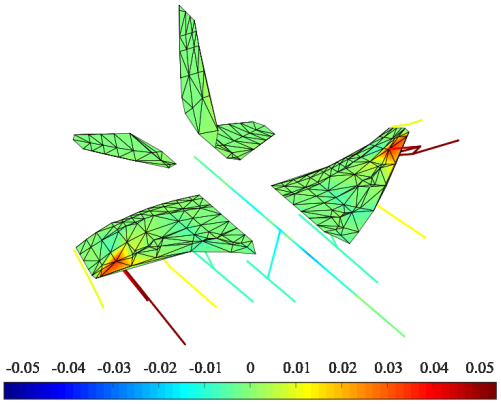


(c) Case 3, TPPC=138.1 W/m

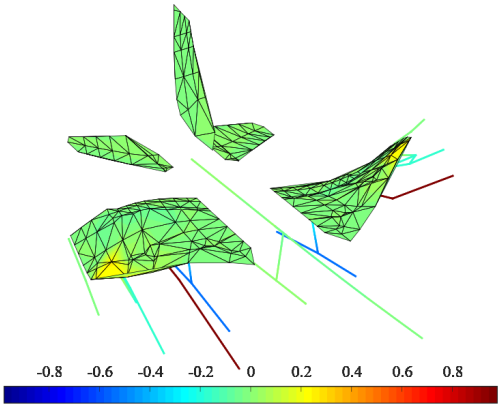


(d) Case 4, TPPC=1057.0 W/m

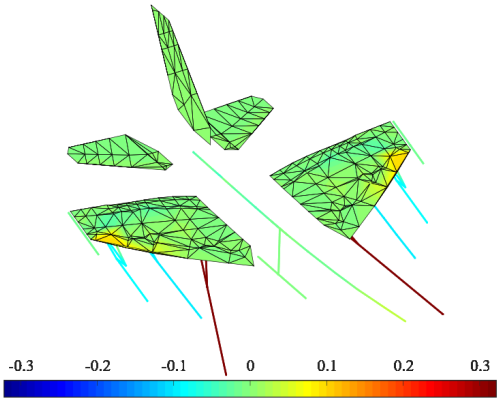


(e) Case 5, TPPC=550.88 W/m

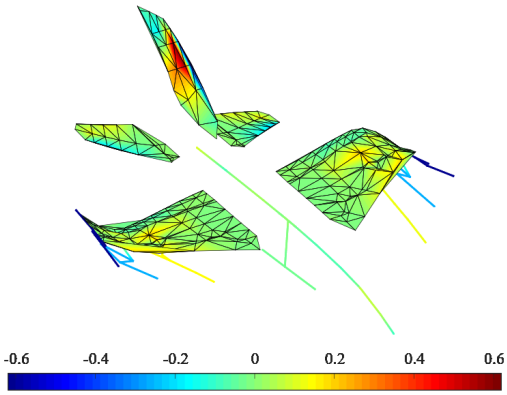


(f) Case 6, TPPC=489.2 W/m

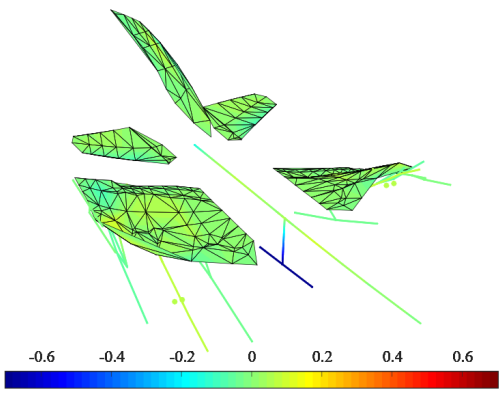


(g) Case 7, TPPC=-176.3 W/m

Figure 3: Visualization of flutter mode deflections and PPC distributions for several flutter test cases

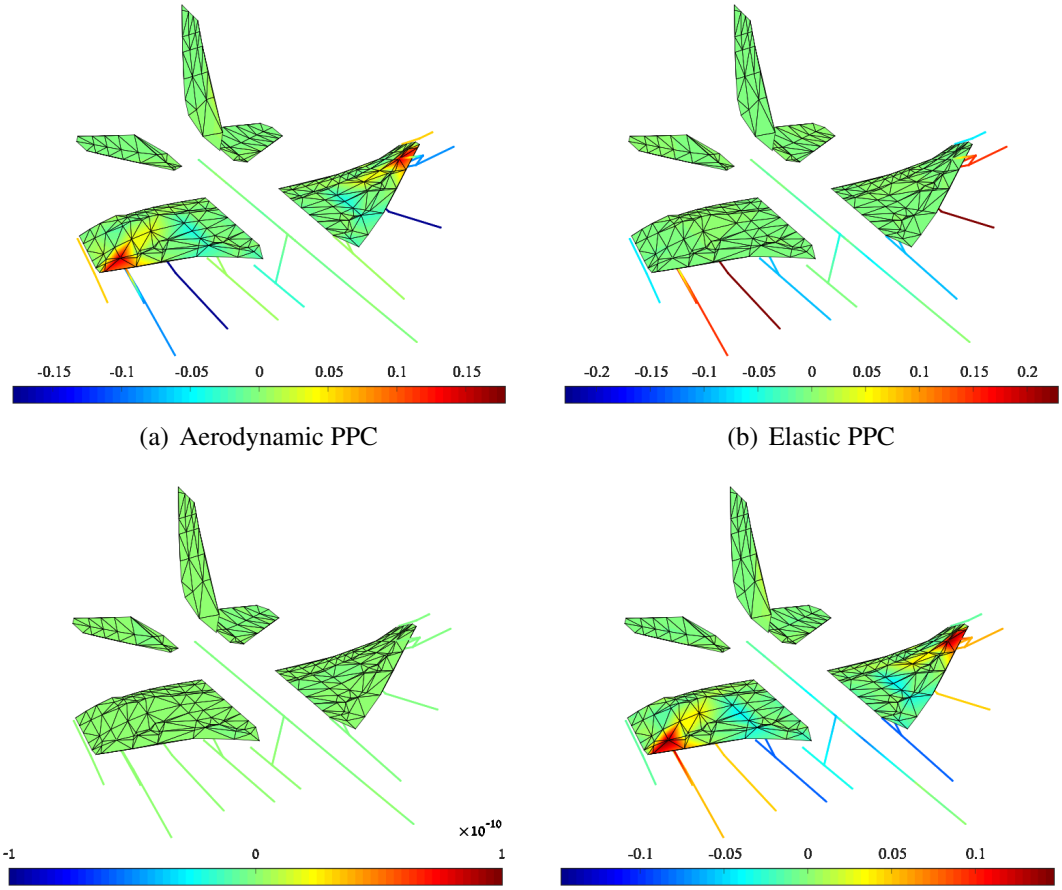


(a) Aerodynamic PPC

(b) Elastic PPC

(c) Inertial PPC

(d) Net PPC

Figure 4: Visualization of flutter mode deflections and aeroelastic energy distribution decomposition into aerodynamic, elastic and inertial contributions, flutter case 1

### 4.2 Basic PPC Patterns Identification - Symmetric Configurations

In this section, aeroelastic energy analysis results of the symmetric configurations dataset are examined in order to identify typical PPC distribution patterns which may be defined and used as flutter mechanism characteristics. The symmetric configurations dataset includes 2592 permutations. Physically or practically irrelevant flutter cases, such as cases which are identified at extremely high flight speeds, are excluded from the examination. This results in a total of 2274 flutter cases - 1031 cases at Mach 0.95 and 1243 cases at Mach 1.2. These cases are typical F-16 wing flutter cases. Figure 5 presents segmentation of the examined dataset flutter cases by dominant PPC contributors among the main wing sections and store stations. For that purpose, a part was identified as a dominant contributor if its relative PPC was higher than 50%. These results indicate that 98.3% of the cases have dominant PPCs at the outboard wing section, while the 4/6, 3/7 and 1/9 store stations are dominant in 13%-24% of the cases. The remaining structural parts are found to be statistically negligible for the purpose of energy distribution characterization. Following these results, the dataset was re-segmented in order to examine the prevalence of flutter cases which are dominated by the outboard wing (OW) PPC or by some combination between the outboard wing and store stations 1/9, 3/7 and 4/6. This examination is presented in Figure 6. According to these results, 98.3% of the dataset cases which have high PPC at the outboard wing section, can be clustered into the 5 most prevalent PPC pattern groups, suggesting that these groups may well characterize any possible F-16 wing flutter case.

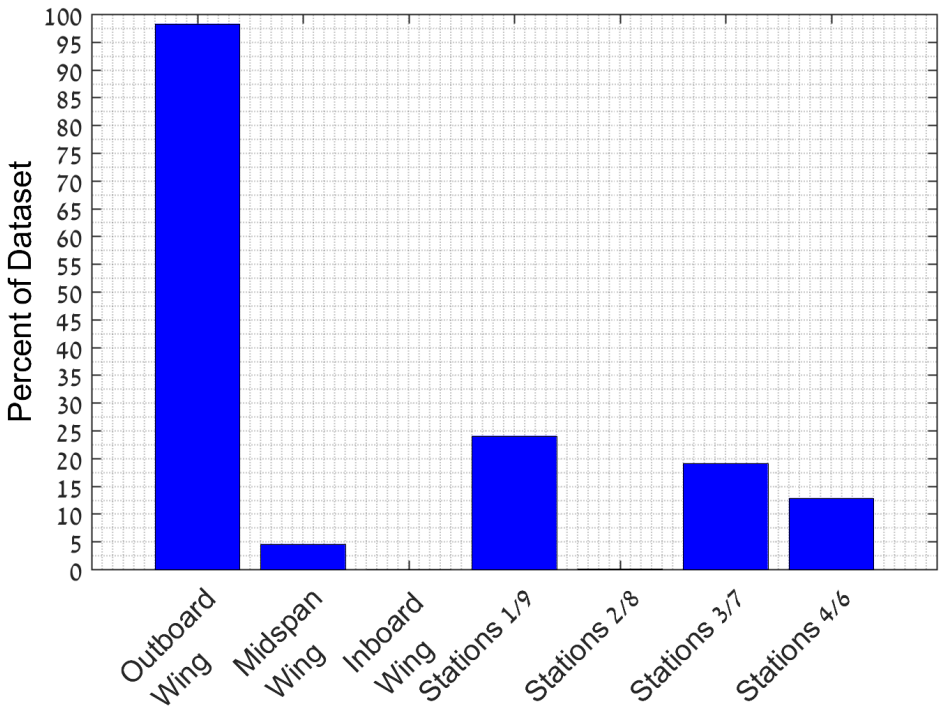


Figure 5: Segmentation of the symmetric configurations dataset

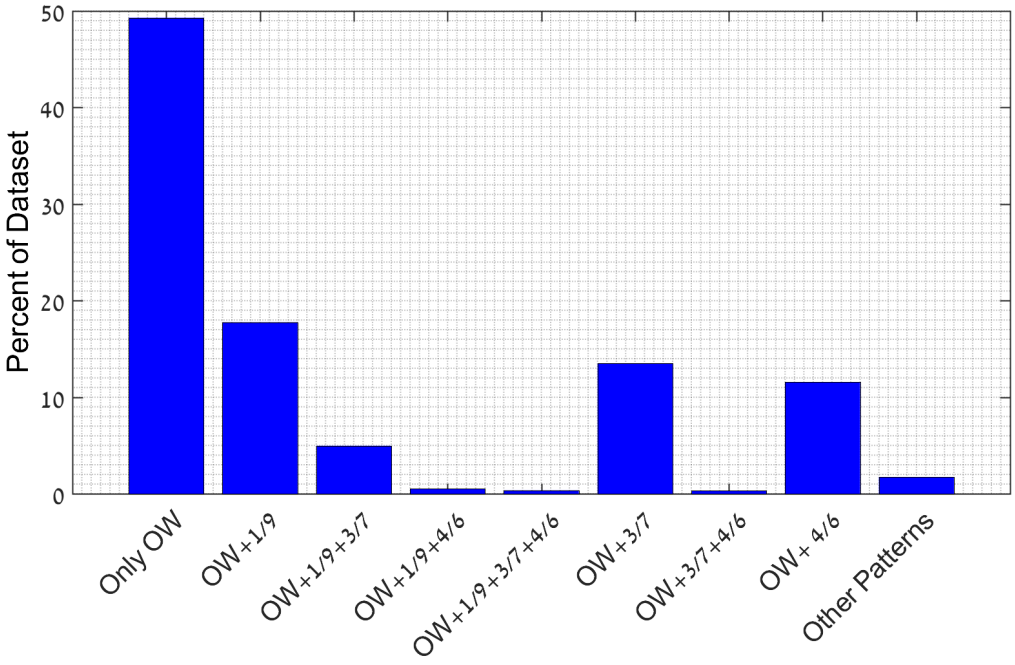


Figure 6: Segmentation of the symmetric configurations dataset

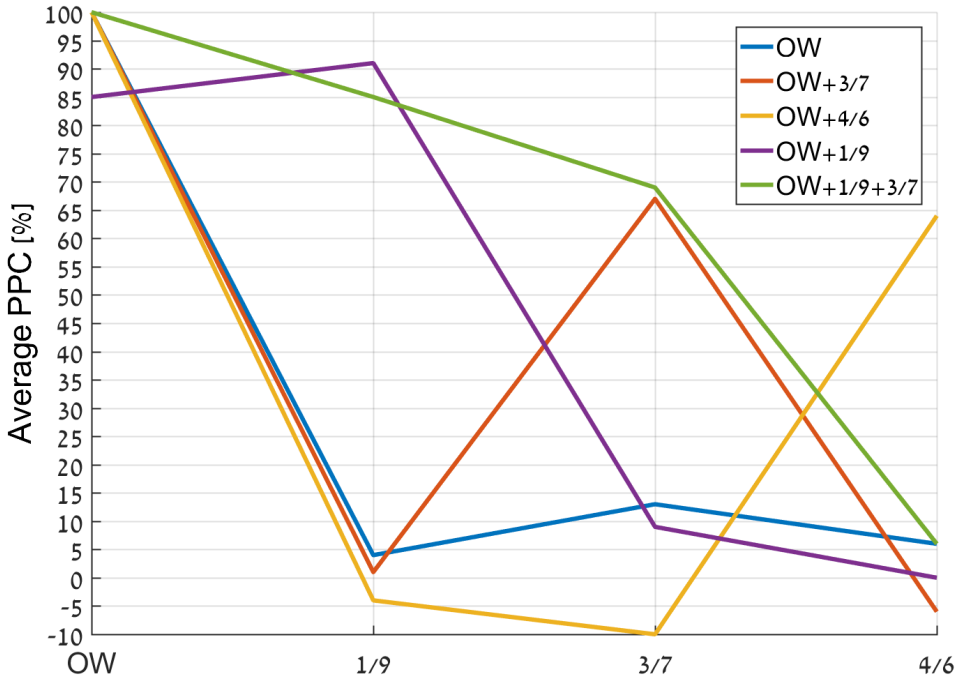


Figure 7: Parallel coordinates representations of the identified groups of symmetric flutter cases

To enable better examination of the results, a parallel coordinates display method is utilized. This method of display allows to visualize high dimensional data, where each observation is represented by the sequence of its coordinate values plotted against their coordinate indices. For the current application, Figure 7 presents average PPCs vs. the OW, 1/9, 3/7 and 4/6 components for the identified five basic pattern groups. In this presentation, the structural components are used as parallel coordinates. From this presentation it is clear that the groups are well distinguished by its dominant PPC contributors. Store stations which are not dominant in a specific group contribute less than 15% of PPC.

Further examination of these groups showed a clear distinction between the groups by flutter case symmetry conditions. Following this observation, Table 4 presents a list of six basic flutter mechanism groups which are identified based on the prevalent PPC pattern groups observed in Figure 6. Most of the OW group cases have anti-symmetric (A/S) conditions, while about 20% of the cases have symmetric (SYM) conditions. The rest of the groups are either A/S or SYM. This set of mechanisms is also reasonable from a physical point of view. The examined dataset includes F-16 wing flutter cases. As suggested in the previous section, high PPC levels at the outboard wing section are typical for every wing flutter case, therefore all F-16 wing mechanisms include considerable contribution of the OW section. Nevertheless, some mechanisms are also significantly affected by the 1/9, 3/7 and 4/6 store stations, since these stations affect the basic wing modes and thereby its flutter characteristics. Consequently, the appearance of the stores-dominant mechanisms is strongly correlated to the dynamic properties of the stores. Mechanisms 3-5 evolve from mechanism 1 as the stores on stations 1/9 and 3/7 become more dynamically significant (i.e. its inertial properties increase). Mechanism 6 evolves from mechanism 2 as the stores on stations 4/6 become more dominant.

| Mechanism | Dominant Component | Symmetry |
|---|---|---|
| 1 | OW | A/S |
| 2 | OW | SYM |
| 3 | OW+1/9 | A/S |
| 4 | OW+3/7 | A/S |
| 5 | OW+1/9+3/7 | A/S |
| 6 | OW+4/6 | SYM |

Table 4: Summary of PPC pattern based mechanism groups

Flutter mode deflections and PPC distributions are presented in Figure 8 for typical cases of the identified mechanisms. For mechanisms which are dominated by the store stations (3-6), significant stores rotation, pitch, swing or yaw motions relative to the wing motion may be observed.

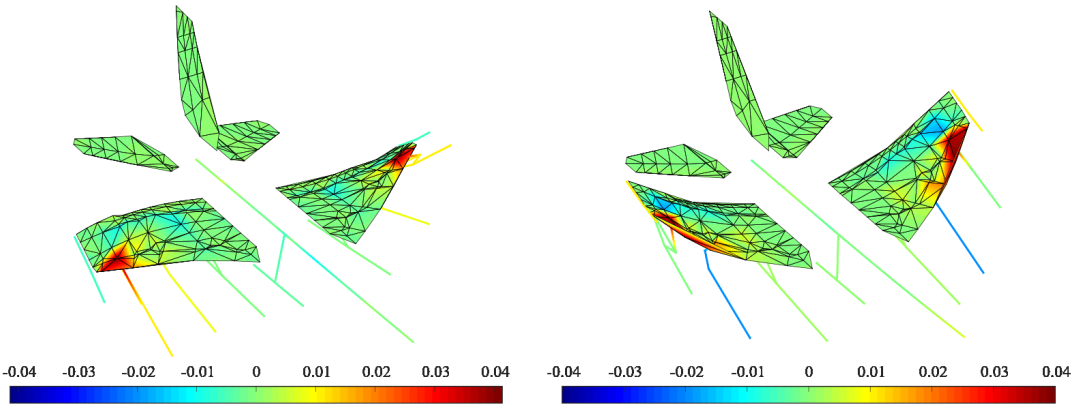


(a) Mechanism 1, OW, A/S (b) Mechanism 2, OW, SYM

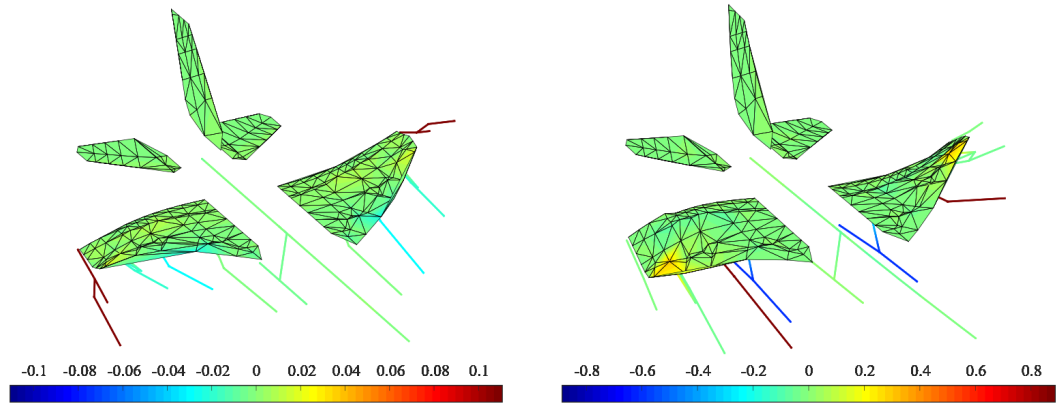


(c) Mechanism 3, OW+1/9, A/S (d) Mechanism 4, OW+3/7, A/S

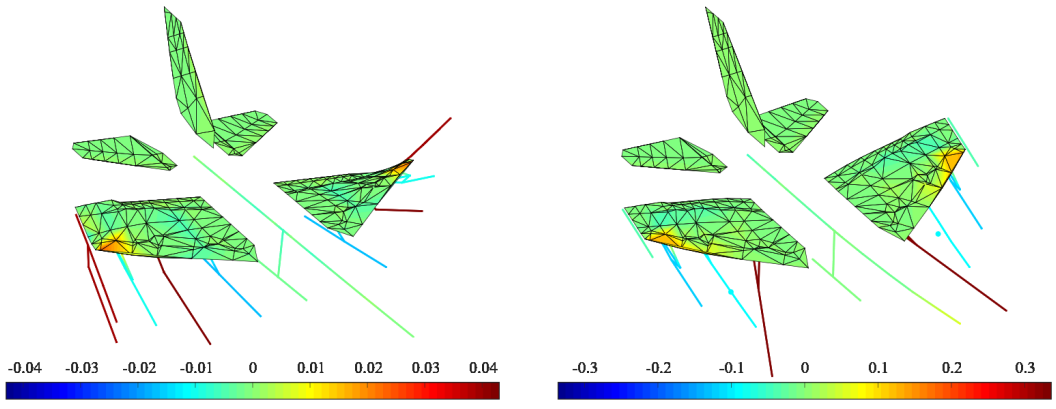


(e) Mechanism 5, OW+1/9+3/7, A/S (f) Mechanism 6, OW+4/6, SYM

Figure 8: Visualization of flutter mode deflections and PPC distributions for typical cases of the identified mechanisms

### 4.3 PPC Patterns Generalization - Asymmetric Configurations

The test dataset contains tens of thousands of asymmetric permutations. In the current section, only first-order asymmetric permutations are considered, that is, symmetric permutations in which only one store was removed from the right wing, leaving the left wing heavier. Analyzing these configurations yielded a total of 7718 flutter cases, 3323 at Mach 0.95 and 4395 at Mach 1.2. These cases are analyzed in attempt to generalize the findings of the previous section to asymmetric flutter cases. Generally, asymmetric flutter cases may be divided into three types: cases in which both wings exhibit similar flutter characteristics (Type 1), cases in which only one of the wings exhibit flutter characteristics (Type 2), and cases in which both wings exhibit dissimilar flutter characteristics (Type 3). Figure 9 demonstrates segmentation of the examined asymmetric cases dataset into these three types based on the PPC patterns identified in the previous section. For that purpose, each wing was individually classified into one of the basic mechanisms identified in the previous section. Cases in which both wings are classified to the same mechanism are identified as Type 1. Cases in which only one of the wings is classified to a mechanism, or if the overall PPC differences between the wings are higher than 20%, are identified as Type 2 with a dominant wing. Cases in which both wings are classified into different mechanisms are identified as Type 3. The presented results indicate that 20.9% of the cases may be classified as Type 1. These cases may be refereed as ”light asymmetry” in which the flutter case mechanism identification is unaffected by the configuration asymmetry. Type 2 group includes 74.5% of the cases, 65.4% of which are characterized with a dominant light wing and 34.6% are characterized with a dominant heavy wing. The remaining minority of cases (4.6%) consist of only 1.7% which are classified as Type 3 and 2.9% which are undetected according to the identified classification criteria. These results are in compliance with the common interpretation of asymmetric flutter cases according to which configuration asymmetry will rarely introduce a new type of mechanism. These results strongly suggest that the basic PPC patterns and corresponding mechanisms which were identified based on the symmetric configurations dataset may be naturally generalized for characterization and classification of asymmetric configurations with only a small percentage of cases (2.9%) remain undetected based on these patterns. Figure 10 presents visualization of typical Type 1, 2 and 3 asymmetric flutter cases.

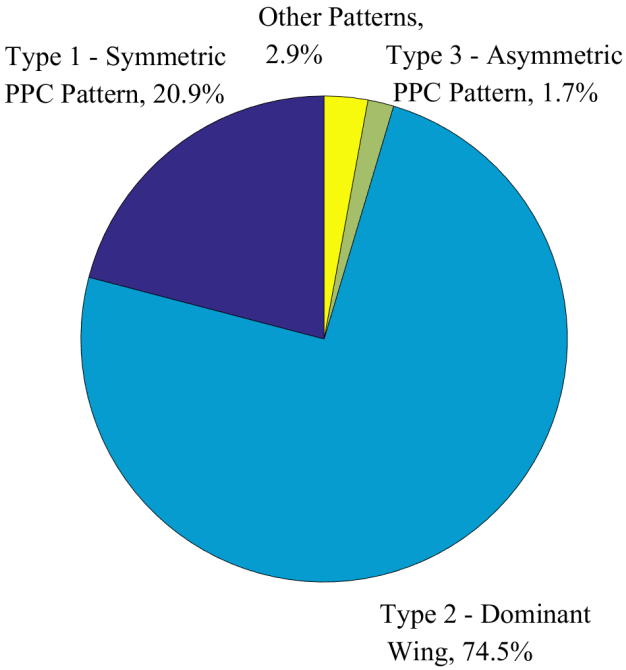


Figure 9: Asymmetric configurations dataset segmentation by PPC patterns

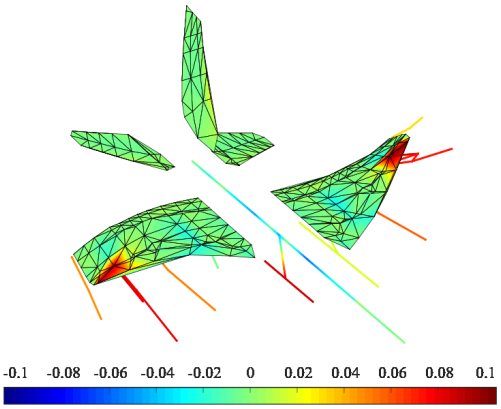


(a) Type 1

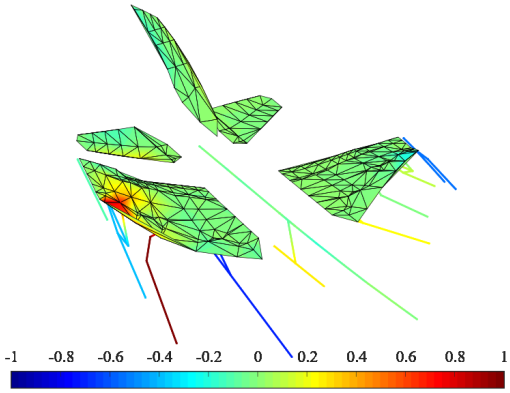


(b) Type 2 - Dominant light wing

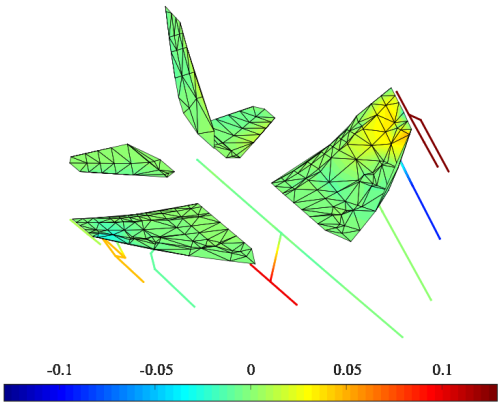


(c) Type 2 - Dominant heavey wing

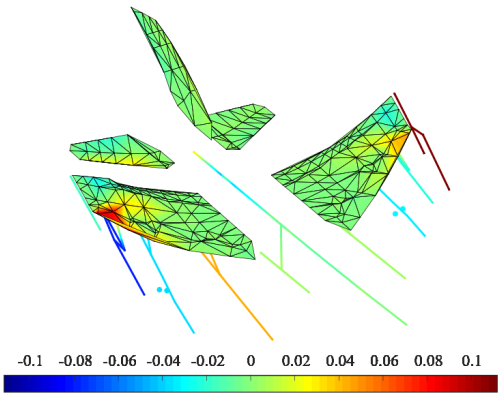


(d) Type 3

Figure 10: Visualization of flutter mode deflections and PPC distributions for typical asymmetric type cases

## 5 SUMMARY AND DISCUSSION

This work studies the applicability of aeroelastic energy distribution analysis for the purpose of enhanced characterization and automated classification of typical flutter analysis results. The study is focused on wing flutter characteristics of a fighter aircraft with multiple external stores which raises practical challenges in typical flutter certification activities of such a platform.

The study suggests a straightforward derivation of aeroelastic power per flutter mode cycle parameters which is formulated in the structural model coordinates and thereby may be easily computed and visualized as part of a typical flutter analysis framework. Power per cycle calculations enable to determine the severity of a flutter case and thereby to identify false flutter cases. Using the suggested approach, a representative dataset of thousands of wing flutter cases of the F-16 aircraft with various stores was examined and basic patterns of aeroelastic power per cycle distributions were identified. These patterns enable to distinguish between wing flutter cases which are dominated by the wing itself and cases in which specific store stations significantly contribute to the destabilizing energy balance of the configuration. Based on these patterns, six basic flutter mechanism groups are identified in the examined dataset. It was shown that 98.3% of the examined symmetric configuration cases can be automatically classified into one of these mechanism groups. A similar classification concept was applied to the asymmetric configurations dataset with similar successful detection rates.

Overall, the suggested analysis approach shows high potential for determining flutter severity along with characterization and automated classification of flutter mechanisms, which may significantly reduce the workload during a typical flutter certification process. Furthermore, evaluation of power per cycle distribution patterns may aid in identification of the main structural contributors to the unstable coupling and thereby offers an insightful information for the analyst.

In future studies, aeroelastic energy analysis concepts may be applied to other aeroelastic applications such as dynamic loads and aeroservoelasticity.

## 6 REFERENCES

[1] Chipman, R. R. and Malone, J. B. (1976). Study Of A Method For Determining Critical Store Configurations For Wing-Store Flutter. Tech. Rep. ADCR-76-1, Naval Air System Command.

[2] Livshitz, A. and Iovnovich, M. (2016). An Artificial Neural Network Approach to Flutter Mechanism Classification. In *56th Israel Annual Conference on Aerospace Sciences*. Tel-Aviv, Israel: Faculty of Aerospace Engineering, Technion, Israel. WeL2T4-01.

[3] Ricciard, A. P. (2017). Aeroelastic Energy Analysis Using Distributed Aerodynamic Work Visualization. *AIAA Journal*, 55(6), 2113–2117. doi:10.2514/1.J055677.

[4] Gu, Y. and Yang, Z. (2012). Modified p-k Method for Flutter Solution with Damping Iteration. *AIAA Journal*, 50(2), 507–510. doi:10.2514/1.J051360.

[5] ZONA Technology, Scottsdale, AZ (2016). *ZAERO, Ver. 9.2, Theoretical Manual*.

## COPYRIGHT STATEMENT